Journal of Biotechnology 383 (2024) 27–38

Contents lists available at ScienceDirect

Journal of Biotechnology

journal homepage: www.elsevier.com/locate/jbiotec

RNA-based detection of genetically modified plants via current-voltage characteristic measurement

Chun-Kai Huang [a,b,c], Yi-Nan Lin [a,b], Wen-Shan Huang [a,b], Satyajyoti Senapati [d], Hsueh-Chia Chang [d], Yi-Ming Sun [b,e], Li-Fen Huang [a,*]

[a] Graduate School of Biotechnology and Bioengineering, Yuan Ze University, Taoyuan 320315, Taiwan, Republic of China
[b] Department of Chemical Engineering and Materials Science, Yuan Ze University, Taoyuan 320315, Taiwan, Republic of China
[c] Institute of Plant and Microbial Biology, Academia Sinica, Taipei 115201, Taiwan, Republic of China
[d] Department of Chemical and Biomolecular Engineering, University of Notre Dame, Notre Dame, Indiana 46556, United States
[e] R&D Center for Membrane Technology, Chung Yuan University, Taoyuan 320071, Taiwan, Republic of China

ARTICLE INFO

Keywords:
Anion-exchange membrane
Current-voltage characteristics
Hygromycin phosphotransferase
RNA
Transgenic plants

ABSTRACT

The widespread adoption of genetically modified (GM) crops has escalated concerns about their safety and ethical implications, underscoring the need for efficient GM crop detection methods. Conventional detection methods, such as polymerase chain reaction, can be costly, lab-bound, and time-consuming. To overcome these challenges, we have developed RapiSense, a cost-effective, portable, and sensitive biosensor platform. This sensor generates a measurable voltage shift (0.1–1 V) in the system's current-voltage characteristics, triggered by an increase in membrane's negative charge upon hybridization of DNA/RNA targets with a specific DNA probe. Probes designed to identify the herbicide resistance gene hygromycin phosphotransferase show a detection range from ~1 nM to ~10 μM and can discriminate between complementary, non-specific, and mismatched nucleotide targets. The incorporation of a small membrane sensor to detect fragmented RNA samples substantially improve the platform's sensitivity. In this study, RapiSense has been effectively used to detect specific DNA and fragmented RNA in transgenic variants of Arabidopsis, sweet potato, and rice, showcasing its potential for rapid, on-site GM crop screening.

1. Introduction

Genetically modified (GM) crops are engineered to obtain beneficial traits such as resistance to herbicides, pests, or diseases, increased yield potential, and improved nutritional contents (Benbrook, 2016; Beyer, 2010; Tripathi et al., 2007; Wang et al., 2019). Numerous studies have shown the benefits of GM crops, including the ability of disease-resistant GM papaya and pest-resistant GM eggplant to help farmers and industries in combating infestations (Shelton et al., 2018; Tripathi et al., 2007), and the provision of vitamin A through Golden Rice to over 250 million children with vitamin A deficiency (Beyer, 2010; Ye et al., 2000). Collectively, the meta-analysis confirmed that GM crops bring about significant improvements in yield gains and nutrient acquisitions (Klumper and Qaim, 2014).

Despite the benefits that GM crops have brought to human, concerns about their safety and potential risks continue to grow with advancements in agricultural biotechnology. Hygromycin phosphotransferase (HPT) and neomycin phosphotransferase II are commonly used as positive selection markers for plant transformation to obtain hygromycin and kanamycin resistance, respectively (Miki and McHugh, 2004). There is rare evidence of horizontal transfer of transgenic plant DNA or antibiotic-resistance genes from GM foods to microorganisms and animals, including humans (Nielsen et al., 1998; Philips et al., 2022; Un Jan Contreras and Gardner, 2022). In addition, transgenic crops expressing Cry toxins derived from *Bacillus thuringiensis* have been introduced to control specific target pest species such as Lepidoptera pests; however, non-target pests and mammals may also be affected (Babin et al., 2020; Marvier et al., 2007; Rubio-Infante and Moreno-Fierros, 2016). Glyphosate is an herbicide widely used for weed management in conjunction with the cultivation of glyphosate-tolerant crops. Overuse of glyphosate

Abbreviations: GMO, genetically modified organisms; RT-PCR, reverse transcriptase-polymerase chain reaction; AEM, anion-exchange membrane; CVC, current-voltage characteristics; HPT,, hygromycin phosphotransferase; ELISA, enzyme-linked immunosorbent assay.

* Corresponding author.
E-mail address: hlf326@saturn.yzu.edu.tw (L.-F. Huang).

https://doi.org/10.1016/j.jbiotec.2024.02.002

Available online 7 February 2024

creates selection pressure that leads to the emergence of more resistant weeds and soil microbial communities, creating new weed management and environmental concerns (Benbrook, 2016; Ruuskanen et al., 2023). Therefore, GM foods pose potential risks to the health and safety of people, animals, and environment.

Safety, ethical, social, and intellectual property concerns surrounding the use of genetically modified organisms (GMO) technology in food production have sparked debates. It is crucial for consumers to be informed about the presence of GMOs in their food to safeguard their rights, monitor gene contamination in native species, and ensure the purity of imported seeds, grains, and organic products (Mallory-Smith and Zapiola, 2008). A reliable and cost-effective GMO detection method is required to achieve this. However, conventional methods for detecting transgenes are expensive, require laboratory operations, or have low sensitivity. Several diagnostic methods have been developed to protect the rights of customers to ensure the detection of transgenes in foods or the purity of imported seeds. One of these detection methods is the polymerase chain reaction (PCR). This method involves amplifying specific DNA sequences of transgenes in GM foods by detecting specific PCR products or instantly measuring fluorescent signals using various strategies, including real-time reverse transcription PCR (RT-PCR) (Randhawa et al., 2009). Despite its high sensitivity and accuracy, PCR can be costly because it requires specialized equipment and skilled technicians. Enzyme-linked immunosorbent assay (ELISA)-based detection methods, including immunostrips, require specific antibodies to detect specific proteins expressed by GMOs (Dong et al., 2019; Zhang et al., 2016). ELISA is more cost-effective and versatile than PCR; however, it involves using patented procedures or specific antibodies and might produce inaccurate results.

Recently, several DNA hybridization-based biosensors have been developed and emerged as viable alternatives. These biosensors utilize the intrinsic electrochemical properties of a DNA sequence paired with its complementary sequence to offer fast, high sensitivity, real-time detection, and can be used for both laboratory and field applications (Alizar et al., 2014; Chuang et al., 2020; Gao et al., 2022; Garcia-Martinez et al., 2011; Phuong, 2015; Ramshani et al., 2021; Senapati et al., 2014; Sorgenfrei et al., 2011; Taller et al., 2015; Wu et al., 2016). Several specific transgenes were selected as targets, including the *bar* and *nptII* genes, *35S* promoter, nopaline synthase terminator (*NOSt*) to detect GM crops (Wu et al., 2016). Various electrochemical biosensors have been used to detect GM components. Gao et al. established a label-free electrochemical impedance DNA sensor using gold carbon dots to detect transgenic soybean and maize, and their detection of its complementary target DNA had a linear range of 1.0×10^{-7} to 1.0×10^{-13} M (Gao et al., 2022). The gold nanoparticle (AuNP) DNA biosensor measures the changes in the current signal caused by the DNA hybridization event with its target complementary DNA, and this sensing platform has a linear target DNA detection range of 2.0×10^{-7} to 2.0×10^{-12} M (Alizar et al., 2014). However, similar to other electrochemical sensors, significant sample pretreatment is necessary to remove interfering redox agents, thereby preventing their use in the field. Several other DNA sensors have been developed to detect GM components, including carbon nanotube-based (Sorgenfrei et al., 2011), quartz crystal microbalance-based (Garcia-Martinez et al., 2011), field-effect transistor-based DNA biosensor (Phuong, 2015). Although highly sensitive, the consistency and specificity of many are questionable. All these methods require extensive sample preparation, expensive equipment, and reagents. Hence, they are not suitable for point-of-care applications because of their lengthy processing time, high sensor and equipment costs, complicated operation, and the need for highly skilled personnel. To address these issues and to allow robust detection of untreated samples, an anion-exchange membrane (AEM) based nucleic acid sensor was developed by detecting ionic current through the membrane that does not involve electron-transfer reactions, and are therefore not sensitive to redox agents in the sample (Senapati et al., 2014). The change in the ion current-voltage characteristic (CVC) curve due to hybridization of complementary target DNA yields a reproducible standard curve with a linear detection range between 1.0×10^{-6} to 3.0×10^{-11} M (Chuang et al., 2020), which is sufficiently sensitive for most GM detection applications but is so robust that it has been used for minimally treated plasma samples (Ramshani et al., 2021; Taller et al., 2015). Isolation of the nucleic acid target from fouling proteins is unnecessary because the sensing signal is not sensitive to weakly charged biomolecules such as proteins.

The AEM-based nucleic acid sensing platform is inexpensive and rapid (~1 h), and can detect nucleic acids with high sensitivity (~1 pM) and selectivity, including the ability to differentiate single-base mismatches (Egatz-Gomez et al., 2016; Senapati et al., 2014). This biosensing system includes a microfluidic chip that is composed of an AEM sensing unit, a counter reservoir, and a reference electrode fitting tube (Fig. 1), and a current-voltage measuring system. Two Ag/AgCl reference electrodes were used in conjunction with two platinum electrodes that applied a DC current to detect electrical potential differences (Fig. 1). The working principle of the sensing technique is to monitor the changes in CVC behavior in response to the ion-depleted diffusion layer and a charge-polarized layer formed on the positively charged anion exchange membrane when a particular bias voltage is applied to induce the single-direction ion flux across the AEM (Supplementary Fig. S1) (Lee et al., 2008; Senapati et al., 2014; Slouka et al., 2013). The AEM biosensor generates CVC in three regions: ohmic (or underlimiting), limiting, and over-limiting (Supplementary Fig. S1A). At low voltages, the ohmic region follows Ohm's law. The limiting region occurs when the selective transport of negative ions across the AEM creates an ion depletion zone (Supplementary Fig. S1B), resulting in a sudden decrease in the slope of the CVC slope. The voltage drop is then localized to the thin ion-depleted diffusion layer, where the target molecules hybridize with their probes, amplifying the charge signal of the targets. With further increase in voltage, microvortices disrupt the ion depletion zone due to the appearance of an unstable charge-polarized layer, thus increasing the ion current owing to replenishment of the ion-depleted region with the bulk electrolyte by the electroconvective instability of the overlimiting region (Chang et al., 2012). The overlimiting region also exhibits an increased current as a result of water-splitting, which generates new H^+ and OH^- ions. When additional negatively charged DNA/RNA molecules attach to the membrane, they hinder electroconvection and increase the voltage threshold for the establishment of a polarized layer, leading to greater displacement of the CVC (Sensale et al., 2021) (Supplementary Fig. S1C).

In this study, we developed a portable biosensor based on the AEM technology to detect the presence of transgenes in GM plants. Compared to conventional methods like PCR, our biosensor offers faster and more cost-effective detection. The biosensor uses DNA probes for detecting *HPT* transgenes and has a quantifiable dynamic range of 1.0×10^{-5} to 1.0×10^{-9} M for complementary target DNA detection, and a high specificity for differentiating non-specific targets. In addition to the transgene DNAs, the developed sensor successfully detected the presence of transgene with improved efficiency using fragmented RNAs of sweet potato, Arabidopsis or rice as inputs. Overall, we developed a promising, easy-to-operate biosensor that is portable, rapid, and low-cost for detecting transgenes in GM plants.

2. Materials and methods

2.1. Probe design

We designed 20-base long probes (Supplementary Fig. S2) to detect the *HPT* gene, a widely used selection marker for plant transformation. Probe specificity was confirmed using the basic local alignment search tool (BLAST, NCBI) by comparing probe sequences with the genome sequences of *Arabidopsis thaliana*, *Ipomoea batatas* (sweet potato), and *Oryza sativa* (rice). The *HPT* gene sequence was obtained from the binary vector pCAMBIA1301 (accession number: AF234297, NCBI). Probes

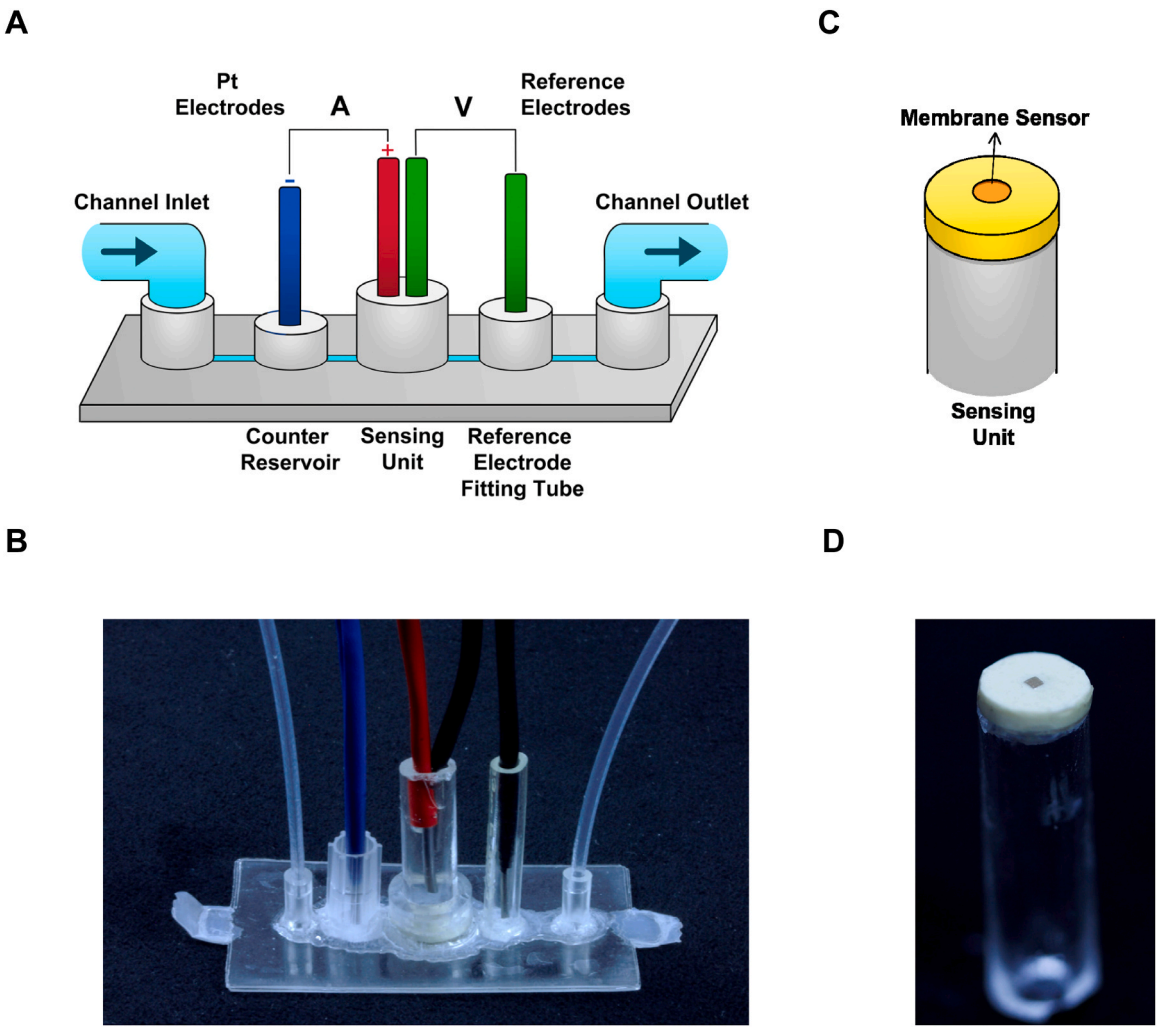

Fig. 1. Schematics of the nucleic acid-detecting biosensor system. (A) Simplified diagram of the microfluidic sensor chip with two paired electrodes. The chip consists of four parts, a single flow channel (light blue), a sensing unit, a counter reservoir, and a fitting tube for the reference electrode. The flow channel has both an inlet and an outlet for nucleic acid sample loading and subsequent PBS buffer washing. The sensing unit has a membrane sensor functionalized with specific probes facing downward to detect nucleic acids in the flow channel. The platinum electrode pair (red and blue) was used to apply the current load across the membrane sensor, and the Ag/AgCl reference electrode pair (green) was used to measure the resulting potential across the nanomembrane sensor to obtain the current-voltage characteristics plot. (B) A photo of the microfluidic sensor chip showing two paired electrodes and the connected tubing. (C) A schematic representation of the sensor unit made by embedding a small piece of anion exchange membrane into polyurethane resin and attaching it to a short piece of plexiglass tubing. (D) A photo of the sensor unit showing the embedded membrane on top.

with varying GC contents were designed (Supplementary Fig. S2) and ordered from Integrated DNA Technologies. Melting temperatures were calculated using an online Oligo Calc (http://biotools.nubic.northwestern.edu/OligoCalc.html).

2.2. Microfluidic chip design and construction

The microfluidic chip consisted of a single channel, a counter reservoir, a sensing unit, and a reference electrode fitting tube (Slouka et al., 2015) (Figs. 1A, 1B). Four functional units were fabricated from three layers of polycarbonate thermo-softening plastic cut using a Plotter Graphtec 7000 (dimensions: ~25 × 50 × 1 mm^3) and sealed together using heat and pressure bonding. Plexiglass was cut and glued to the polycarbonate chip using UV curing Acrifix 192 to build a counter reservoir and reference electrode fitting tube. The primary sensor disk, designed using computer-aided design (CAD), was 3D printed as a template to create a silicone mold for further sensor disk generation. The sensor was fabricated by embedding a small piece of an anion exchange membrane (~0.4 or 0.1 mm^2) into polyurethane resin using a fast-curing polyurethane molding protocol, as previously described in (Senapati et al., 2014). After 30 min, a polyurethane-based sensor disk with an exposed sensor membrane was cast and glued to a short piece of plexiglass tubing (Figs. 1C, 1D) using UV curing Acrifix 192. The plexiglass tube was connected electrodes to measure current-voltage signals from the sensor (Figs. 1A, 1B).

2.3. DNA probe functionalization

The DNA probes (Supplementary Fig. S2) were functionalized onto the anion exchange membrane of the sensor using 1-Ethyl-3-(3-dimethylaminopropyl) carbodiimide (EDC) (Sigal et al., 1996) and a carboxyl-terminated photocrosslinker (Lin et al., 1988), following the protocol described in (Senapati et al., 2014). First, COOH groups were formed on the membrane surface through radical polymerization using 10 μL of photoreactive benzophenone-3,3,4,4-tetracarboxylic acid (1 mg in 10 μL water, pH 6–7), followed by UV light exposure (356 nm) at 30 mW/cm^2 for 10 min twice to prevent overheating (ElectroCure 500 UV Chamber, Fusionet, ME, USA). Next, the 5'-amine-coupled DNA probe was covalently attached to the sensing surface using amide linkage by incubating the membrane with 0.4 M EDC in MES buffer for

30 min and an overnight incubation with 10 μM DNA probe in 0.1x PBS solution. The CVC of the sensor membrane before and after functionalization was measured to confirm successful functionalization. Functionalized sensor probes were stored in 0.1x PBS buffer at 4°C before testing.

2.4. Total RNA extraction

Total RNA was extracted from 7-day-old wild-type (WT) and *HPT*-containing transgenic Arabidopsis, sweet potato, and rice seedlings using TRIzol reagent (Invitrogen, MA, USA), following the manufacturer's protocol and treated with RNase-free DNase I (Ambion, MA, USA). These transgenic plants were kindly provided by Dr. Chung-An Lu (Department of Life Sciences, National Central University) (Huang et al., 2015, 2016). Total RNA quality was assessed by analyzing the ratio of 25–18S rRNAs on a 1% agarose gel and quantifying it using a Nanodrop 2000 instrument (Thermo Fisher, MA, USA).

2.5. RNA fragmentation

Total RNA (50 μg) was fragmented using NEBNext magnesium RNA fragmentation buffer (#E6150S, NEB, MA, USA) for 4 min at 94°C and terminated by adding stop solution at 4°C, according to the manufacturer's protocol. Fragmented RNAs were then purified with the Monarch RNA Cleanup kit (T2030, NEB, MA, USA), following the manufacturer's protocol, and eluted with 20 μL DNase/RNase-free distilled water (AM9915G, Invitrogen, MA, USA). Fragmentation yielded RNA molecules approximately 50–100 nt, which were analyzed on a 1.5% agarose gel.

2.6. Measurement of CVC

CVC measurements were conducted using a Gamry 500 potentiostat in a four-electrode setup (Gamry Instruments, PA, USA), as previously described (Senapati et al., 2014). Briefly, a pair of platinum source electrodes were connected to the counter reservoir and the sensor membrane reservoir to apply a DC current, while a pair of silver-silver chloride reference electrodes were positioned in the reservoirs of the sensor membrane and reference fitting tube to measure the voltage responses from the sensor chip as described in (Slouka et al., 2015). A 100 nm pore sized polyvinylidene fluoride (PVDF) membrane (VVLP01300, Merck, Germany) was placed in the counter reservoir base before adding 1% agarose in 0.1x PBS. All reservoirs and channels were filled and equilibrated with 0.1x PBS. The CVCs were obtained by applying a DC current from 0 to 50 μA at a scan rate of 1 μA/sec to measure voltage drop across the sensor membrane. In each experiment, 60 μL of various concentrations of complementary or mismatched antisense DNAs and fragmented RNA samples were loaded into the chip channel and incubated with the sensor for 15 min to allow hybridization. Non-specifically bound DNA/RNA molecules on the sensor membrane surface were washed with 1 mL 4x PBS high-salt solution and equilibrated with 5 mL 0.1x PBS. After removing unbound DNA/RNA fragments, representative CVC curves were recorded to calculate voltage shifts between the blank baseline and sample DNAs/RNAs. The functionalized sensor was regenerated by washing with 0.1x PBS (pH 10) to dehybridize bound nucleotide fragments. Voltage shifts from serial concentrations of antisense DNA were curve-fitted with the equation $\Delta V/\Delta V_{sat} = KC/(1+KC)$, as previously described (Taller et al., 2015), where ΔV is the voltage shift resulted from the presence of antisense DNA concentration (C) in samples, normalized by the maximum saturation voltage shift (ΔV_{sat}), and the affinity constant K is the Langmuir equilibrium constant determined by the curve's slope. This equation was used to determine the target sample concentration.

To verify that the CVC shift in AEM sensor was indeed due to the hybridization of target, we labeled target DNA sequence with fluorescence dye. The fluorescently labeled target DNA solution was then pushed to the chip and incubated for 30 min for hybridization of the target sequence with the DNA probe attached to the AEM sensor (Slouka et al., 2015). The excess labeled DNA was removed using a high-salt 4x PBS solution followed by the measurement of CVC with 0.1x PBS and imaged with a QImaging Retiga 2000R Fast camera under UV illumination in a dark chamber.

2.7. Operation of RapiSense device

The RapiSense is a current-voltage measuring system built by KIB Electronics (Elkhart, Indiana, USA). It features a set of electronic circuits designed to provide a DC current at a rate of 1 μA/sec via a pair of platinum electrodes and to detect voltage responses using a pair of silver-silver chloride electrodes. For ease of use, the RapiSense device includes a connection module to facilitate measurements and digitize the CVC signals, which can then be transmitted to a computer through a USB cable for real-time visualization. The functionalization and measurement operations of the biosensor were consistent with the procedures previously described (Yin et al., 2020).

3. Results

3.1. Effect of immobilized DNA probe on the biosensor response

Nucleic acid sequences are commonly used as probes for biosensor detection, because of their intrinsic ability to bind to their complementary target sequences and form stable double-stranded structures. The efficiency of DNA probe binding depends on the degree of homology between the probe and the target sequence during the complementary binding process. We used several parameters to design the DNA probes (Hendling and Barišić, 2019). First, a probe length of between 20 and 30 bases was considered sufficient for target hybridization specificity (Charlebois et al., 2013; Suzuki et al., 2007). Second, to prevent self-secondary structure formation by the probe and inhibit further complementary binding, the designed probe should have a reduced complementary interval (Wetmur, 1991). Third, multiple iterations of the same base (≤ 4) should be avoided to minimize the risk of false positives. The *HPT* gene is commonly used as a marker in transgenic plant selection. Therefore, we designed four oligo probes with different GC contents to test the efficiency of *HPT* transgene detection. The *HPT* sequence from pCAMBIA1301 was used as a template to design four complementary oligoprobes A, B, C, and D with GC contents of 29%, 48%, 75%, and 70%, respectively (Supplementary Fig. S2), and their melting temperatures (Tm) were 44.6°C, 48°C, 62°C and 60°C, respectively.

On the AEM sensor (Fig. 1), DNA probe A was functionalized using the EDC solution described in the Materials and Methods section, and the target DNA fragment was conjugated with the fluorescent molecule fluorescein amidites (FAM) to visualize the ability of the DNA oligo probe to capture its complementary target (Fig. 2A). The FAM-conjugated target DNA was incubated with the sensor membrane functionalized with probe A (bright-field image in Fig. 2B-i), followed by washing (Fig. 2B-ii and -iii) to remove unbound ssDNA. After washing, the FAM-conjugated target DNA was clearly observed on the sensor membrane (Fig. 2B-iv), indicating that the DNA oligo probe on the sensor membrane could efficiently capture its target DNA fragment.

3.2. Detection kinetic and standard curve of membrane biosensor

An external concentration polarization phenomenon develops on the membrane surface due to imbalanced migration of ions through the ion-exchange membrane under an applied electric field. Consequently, one side of the membrane becomes ion-depleted and the other side becomes ion-enriched. Although charged analytes are associated with the probe and target DNAs, they remain immobile and hence cannot contribute to the ion current flux through the membrane. However, the depletion

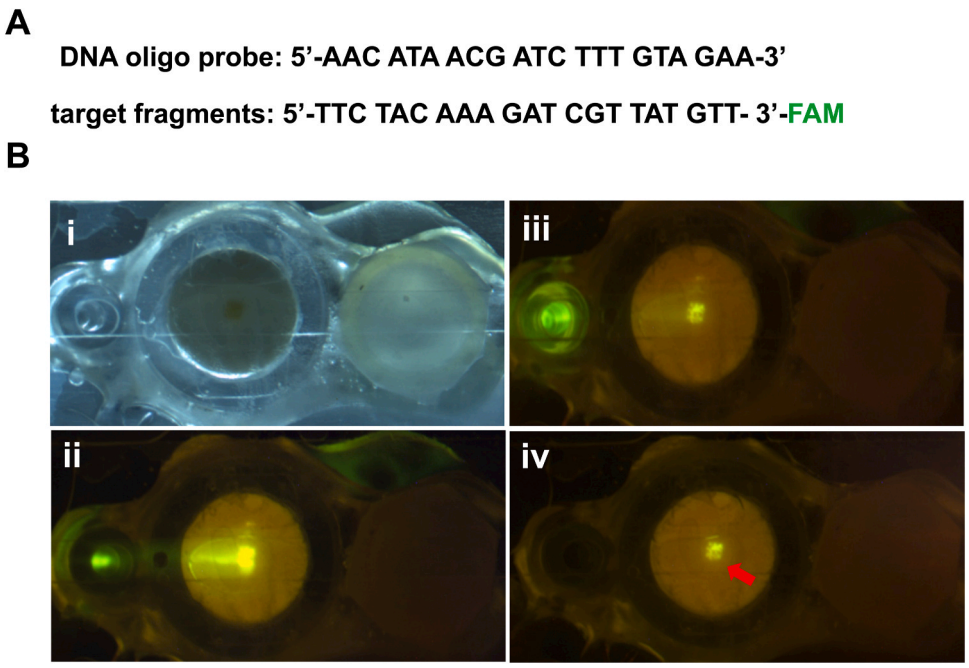

Fig. 2. Specific DNA fragments binding with membrane sensor probe. (A) Sequences of DNA oligo probe and its targeted complementary fragment. The target fragment is covalently conjugated with a FAM fluorescent molecule. (B) Binding of FAM-conjugated single strand target DNA on the sensor membrane. Single strand target DNA (10 nM) was hybridized to the functionalized sensor membrane, following the standard assay procedures. (i-iv) Washing procedures to remove unbound fluorescent single strand DNA target, and fluorescent DNA target was bound on the sensor membrane after the washing procedure (indicated by an arrow).

becomes very severe at sufficiently high voltages, which results in a negative field that draws ions from the bulk solution to maintain the current in the system. This phenomenon is illustrated in Supplementary Fig. S1. The increase of voltage shift is proportional to the net negative charge on membrane surface by the probe-target nucleic acid hybridization from the resulting increases in voltage thresholds for ion entry into the membrane (Sensale et al., 2021). Progressive absorption of the complementary target DNA on the sensor membrane was described using the Langmuir adsorption model (Do, 1998). Because the sensitivity of each membrane sensor device may vary due to differences in fabrication and membrane surface topology, a universal calibration curve can be constructed by normalizing voltage and current measurements using the saturation voltage shift ΔV_{sat} and the critical concentration, which is inversely proportional to the Langmuir constant (Taller et al., 2015).

Probe A was applied (Fig. 3A) to establish the calibration curve to measure the relationship between the concentrations of complementary target A and voltage shifts (ΔV), as depicted in Figs. 3B and 3C. The CVC curve measured at zero concentration of target A was used as the baseline CVC for the zero-shift voltage (V_0), following the standard procedures outlined in the Methods section. We then collected a series of voltage shifts ($\Delta V = V_{measured}-V_0$) in the over-limiting region by applying a range of concentrations (8 nM, 80 nM, 800 nM, 1.6 μM, 8 μM, and 16 μM) of target A (Fig. 3C). Among these concentrations, we found that the voltage shifts after incubation with 8 μM and 16 μM of target A were identical, indicating saturation of the sensor. This voltage shift at the saturation concentration is represented as ΔV_{sat} (ΔV_{sat} = 0.55 V in Fig. 3C). We observed no significant voltage shift when target B and target C were incubated with different samples (Fig. 3B), indicating the high specificity of the probe A sequence for target A. To assess the theoretical relationship between the concentrations of the target DNAs and voltage shifts, we collected data from seven different membrane sensors, as shown in Fig. 3D. Owing to heterogeneity in the AEM, the hybridization equilibrium constant various from sensor to sensor. Using the Langmuir adsorption calibration equation ($\Delta V/\Delta V_{sat} = KC/(1+KC)$) described in Taller et al., 2015 (Taller et al., 2015), we obtained the equilibrium association constant K by finding the slope between two points in the dynamic range from each membrane sensor. The collapsed normalized data are presented in Fig. 3E, showing a linear dynamic range spanning three orders of magnitude, calculated by fitting a curve to the calibrated linear and saturation regions and measuring the concentration at which they intersect relative to the limit of detection. A high level of consistency ($R^2 = 0.9903$) was observed between the data points obtained from 5 different membrane sensors and the calibration curve. This indicated excellent agreement with the Langmuir absorption model, as previously described (Taller et al., 2015), and with the experimental results. Furthermore, the results suggested that the variations arising from each batch of membrane sensors, such as differences in membrane homogeneity and fabrication efficiency, can be minimized after determining ΔV_{sat} and the Langmuir constant K.

In addition, we conducted experiments to study the impact of different GC contents in probes (probe B, C, and D) on the detection of their complementary target DNA, the characteristics of the CVC curve, and the detection sensitivity. Supplementary Fig. S3-S5 provided details of these investigations. Probe C exhibited two palindromic sequences (TGCA and CGGCCG) (Supplementary Fig. S3A), potentially leading to its inability to provide distinct responses across varying concentrations of the complementary target C DNA (Supplementary Fig. S3B). Both sensor probe B and probe D exhibited integral CVC behaviors, enabling them to distinguish between different concentrations of their complementary target DNAs without exhibiting non-specific binding (Supplementary Fig. S4B-C, S5B-C). Similar to the probe A membrane sensor, the ΔV_{sat} of probe B and probe D was ~0.5 V. Furthermore, the linear dynamic range of probes B and probe D spanned three orders of magnitude, and both probes displayed well-calibrated curves with a high level of consistency ($R^2 = 0.9529$ for probe B and 0.9795 for probe D) (Supplementary Fig. S4D and S5D). Based on these results, we propose that this membrane sensor detection system can be optimally employed across a wide range of GC contents within sensor probes. Furthermore, to ensure optimal performance, avoiding palindromic sequences in the design of these probes is recommended.

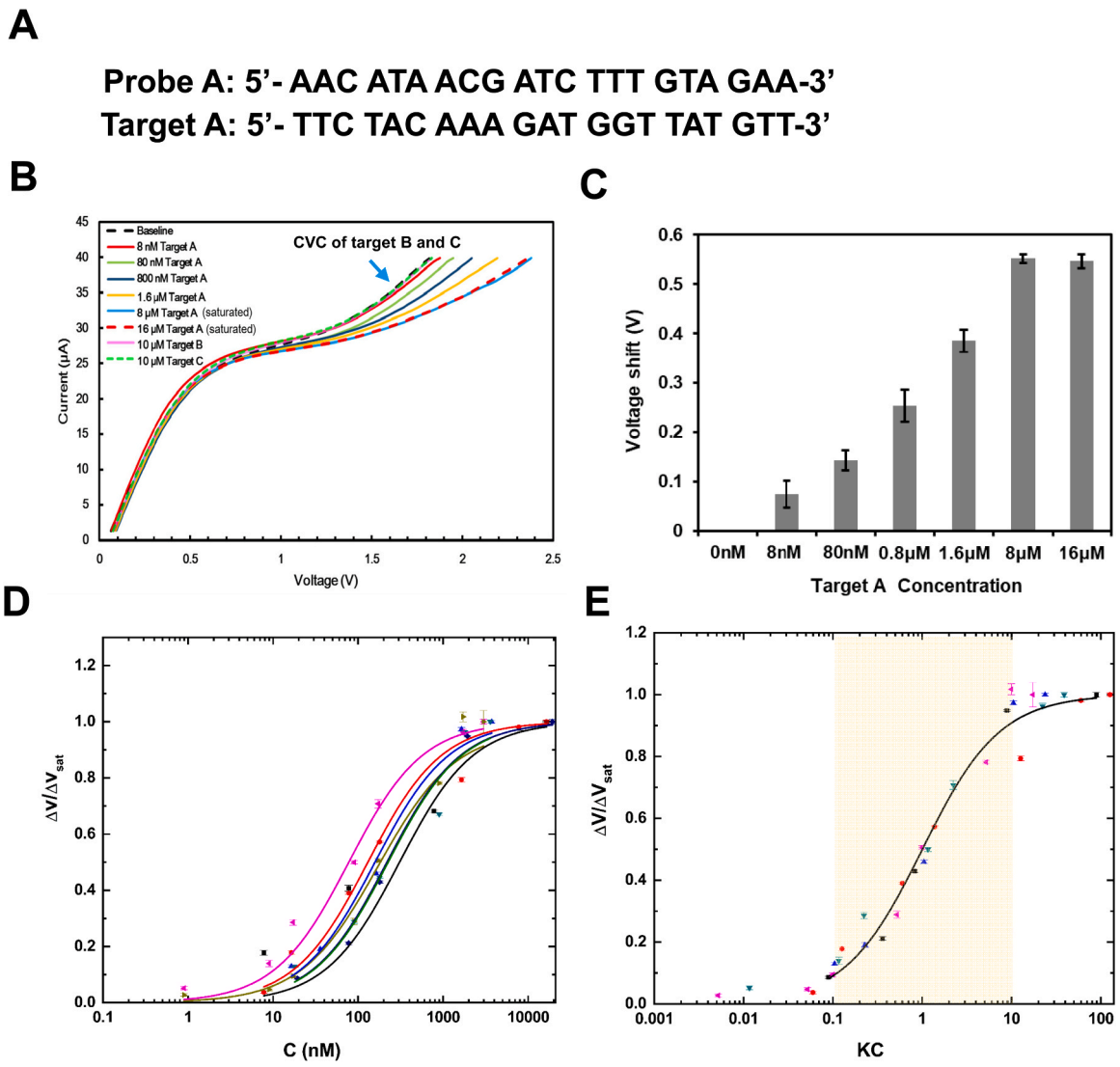

Fig. 3. Specificity and dynamic range of probe A membrane sensor. (A) Sequences of probe A and its complementary target A. Probe A sequence was designed specifically to complement the sequence of hygromycin resistant gene. (B) Representative current–voltage characteristics of probe A conjugated membrane sensor in detecting a series concentration of single strand DNA target A, and non-complementary single strand DNA target B and target C, with buffer only as the baseline. (C) Bar diagram showing voltage shift from probe A with increasing target A concentration. Error bars indicate standard deviations of three replicate experiments. (D) Voltage shift characteristics of seven individually functionalized membrane sensors within a range of target ssDNA concentrations. (E) Universal calibration curve from seven independent membrane sensors with a series of target A concentrations. According to the Langmuir equilibrium model, the data of five probes were normalized by the saturated voltage shift ($\Delta V/\Delta V_{sat}$) as a function of the normalized concentration (KC) (R^2= 0.9903). Each data set was normalized by its maximum saturation voltage shift ΔV_{sat} and the slope of the curve determined the affinity constant K. Shades of grey indicates signals in the linear detection range.

3.3. *Effect of mismatched target DNAs on biosensor detection*

This detection technology depends on DNA hybridization using probe A and its fully matched complementary target A. Almost no voltage shifts were observed when non-complementary targets B and C were applied (Fig. 3). To assess the effect of target DNA with mismatched sequences on this membrane sensor detection system, we designed a series of complementary target sequences with one–three mismatches and avoided secondary structure formation. These complementary mismatched target sequences, with continuous or discontinuous mismatches, were designed at the distal site of the sensor membrane (Fig. 4A). Furthermore, these synthesized mismatched target A (misA1–misA3) were used to elucidate whether probe A could differentiate targets with only a few mismatches from perfect matches. Control experiments were performed by incubation with fully complementary target A and the CVC measurements were repeated. The CVC of the mismatched targets were measured at the saturation concentration of 1 μM (Fig. 4B). Targets with one or two nucleotide mismatches (misA1 and misA2) exhibited ~50% reduction in voltage shifts, whereas targets with three nucleotide mismatches showed ~70% reduction in voltage shifts compared to the control (Fig. 4C).

3.4. *Effect of membrane size on biosensor detection*

We expect to enhance sensor sensitivity by decreasing the size of the sensor membrane, because the sensing principle of the anion-exchange membrane sensor relies on the presence of total negatively charged molecules on its surface. This idea was supported by a study showing that a decrease in the sensor membrane area (3.5–1 mm^2) could improve the detection limit by 4–5 folds (Senapati et al., 2014). Hence, to investigate whether the size of the membrane affected the detection efficiency of the membrane sensor, we fabricated membranes of two sizes, measuring 0.35 mm^2 and 0.12 mm^2 (Fig. 5A). Using a membrane sensor attached to probe A, the voltage shifts generated by target A with

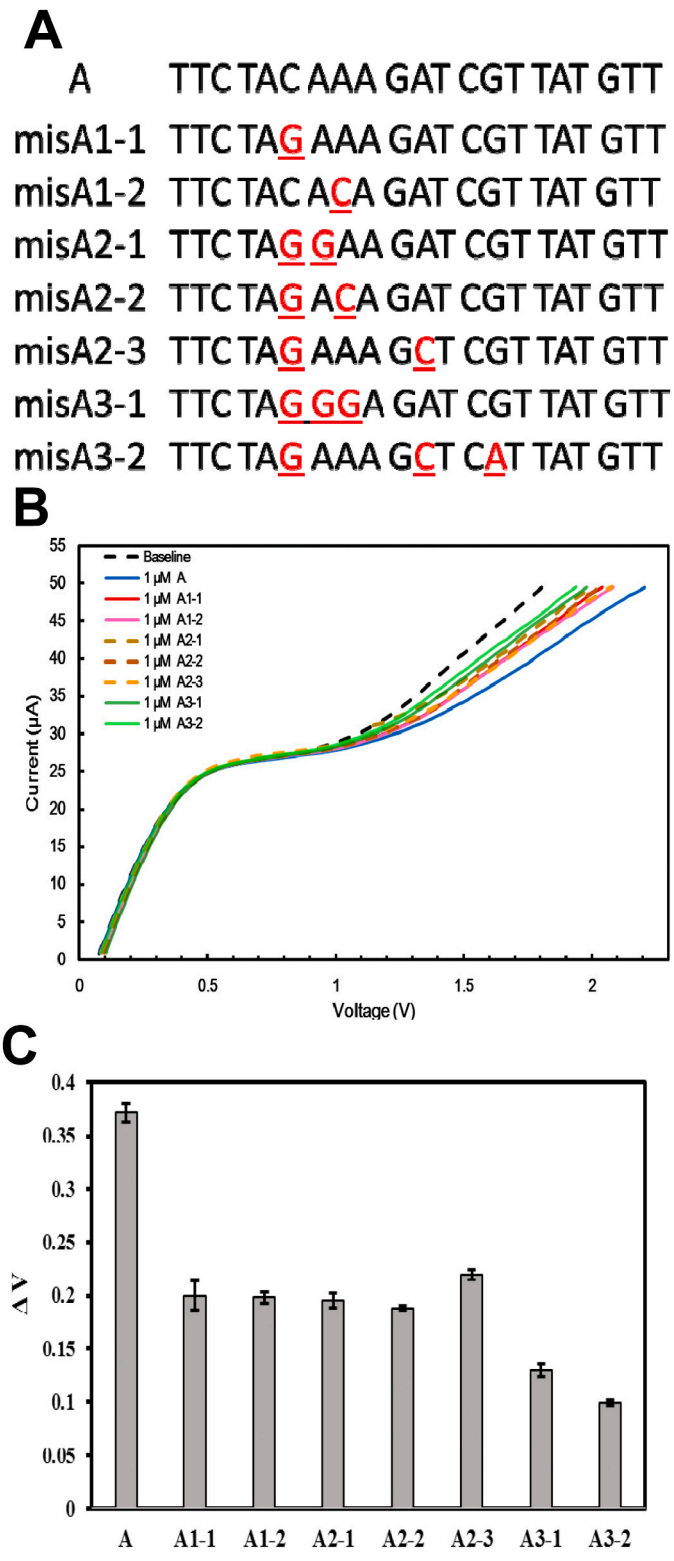

Fig. 4. The effect of mismatched targets on specificity of the membrane sensor. (A) Sequences of target A and a series of mismatched target A1–3 with continuous or discontinuous mismatch nucleotides (labeled in red and underlined) on the distal site to the sensor membrane. (B) Current-voltage characteristics of a series of mismatched target A1–3 with a saturated concentration, 1 μM. (C) Voltage shifts of a series of mismatched target A1–3 with a saturated concentration, 1 μM. Error bars indicate standard deviations of three replicate experiments.

five concentration series were measured and compared with the voltage shift generated by target A at saturated concentrations. Although the two signals were not appreciably different above 10 nM, the smaller sensor allowed a one-log lower detection limit than the larger sensor (Fig. 5B). At 1 nM, only the smaller sensor reported a detectable voltage signal, suggesting that smaller sensors are significantly more sensitive at low target concentrations. The experiment was performed in triplicate, demonstrating the reproducibility of the membrane sensor in consistently detecting low concentrations of DNA after dehybridization and regeneration of the same membrane sensor. Curve fitting of the results in Fig. 5B using the Langmuir equilibrium model showed that the slope patterns of sensors with either a large or a small membrane were similar (Fig. 5C), indicating that the membrane sizes did not affect the characteristics of the membranes, but the detection limit was improved for sensors with a smaller membrane. However, a small sensor membrane may also result in a reduced binding capacity, exhibiting saturation at a lower concentration of the target DNA (Figs. 5B and 5C). Therefore, optimizing the membrane size is crucial for balancing the sensitivity and detection limits of AEM biosensor.

3.5. *RNA Fragmentation of longer RNAs for CVC measurement*

Anion exchange membrane sensors have been previously used to detect target RNAs from various sample sources, such as *Brucella*, *E. coli*, dengue virus, Zika virus, exosome RNA of human or mouse cells, and miRNAs associated with oral cancer (Ramshani et al., 2019; Senapati et al., 2014; Slouka et al., 2015; Taller et al., 2015; Yin et al., 2020). These target RNAs are sufficiently short enough to obtain stable and reliable CVC measurements. The average length of mRNA in eukaryotes is 1–2 kb, which is too long for detection using surface-immobilized probes (Mehlmann et al., 2005). The adverse effects of using longer mRNAs directly for detection include decreased sensitivity owing to the formation of secondary and tertiary structures that blocks recognition, increased time for the probe to scan through long mRNAs, and increased non-specific interactions between the inherent positive charges of the anion exchange membrane and the negative charges of longer RNA molecules to further perturb CVC measurement. Hence, we decided to shorten the lengths of the sample RNAs to enhance sensitivity, decrease hybridization time, and reduce nonspecific binding by RNA fragmentation with magnesium ions at 94℃ (Fig. 6A). To validate the ability of the membrane sensors to detect the mRNA transcripts of transgenes in transgenic plants, we extracted total RNAs from sweet potato and Arabidopsis. The total RNAs were first fragmented into 50–100 nt in size following Mg^{2+}-dependent RNA fragmentation (Fig. 6B) and these fragmented RNAs were used in CVC measurements for detection with the AEM-based biosensors. The measured CVC curves for samples of sweet potato with a hygromycin resistance transgene (sweet potato-Hyg) or transgenic Arabidopsis (Arabidopsis-Hyg) displayed significant voltage shifts were compared to the results of wild-type sweet potato (sweet potato-WT) and wild-type Arabidopsis (Arabidopsis-WT) (Fig. 6C-D). These results indicated that the mRNA transcripts of the *HPT* transgene from transgenic plant samples could be successfully detected using AEM biosensors with properly fragmented RNA samples.

3.6. *A prototype of AEM-based biosensor RapiSense for transgenic plant detection*

Based on the optimized parameters of the AEM-based biosensor detection system, a reliable, cost-effective, and user-friendly GMO detection system, RapiSense, was designed along with a probe-conjugated disposable microfluidic AEM biosensor chip. This system was designed to connect to a personal computer, enabling the control of the RapiSense unit and recording the CVC measurement results (Fig. 7A). Traditional RNA detection methods, such as quantitative RT-PCR, requires ~60 min for the reverse transcription of RNAs into cDNAs plus approximately ~60–90 min for PCR amplification of the reverse

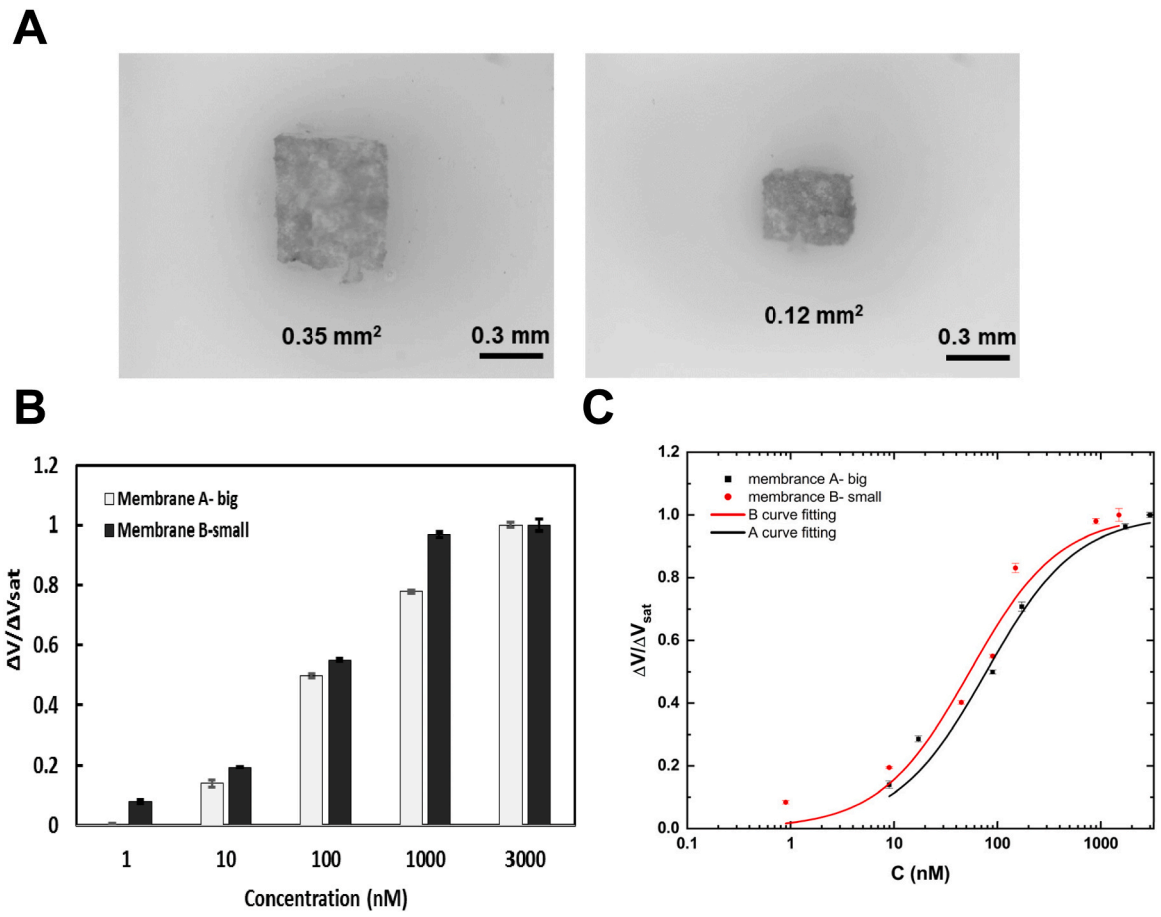

Fig. 5. The effect of membrane size on detection efficiency. (A) The big and small membranes observed under a microscope. (B) The voltage-shift characteristic for depiction of large and small membrane in different target A concentration series. Error bars indicate standard deviations of three replicate experiments. (C) Curve fitting of the results from the two membranes, based on the Langmuir equilibrium model. The same slope pattern indicates that membrane size does not affect the characters of membranes but the sensitivity is increased when membrane size is smaller.

transcribed target cDNAs. In contrast, RapiSense detection required only ~10 min for RNA fragmentation, less than 50 min to wash unspecific binding, and 5 min for target RNA detection (Fig. 7B). Consequently, RapiSense can reduce detection time and enable efficient on-site analyses. To assess its proficiency, the RapiSense was evaluated using varying concentrations of complementary single strand DNA for probe A. The results demonstrated successful detection and the ability to differentiate target DNAs at concentrations ranging from 0.025 μM to 2.2 μM, as evidenced by distinct voltage shifts (Fig. 7C). RapiSense was also further tested using fragmented RNAs extracted from transgenic rice as input. The CVCs of fragmented RNAs extracted from both wild-type and transgenic rice were measured using RapiSense and compared with the CVC baseline. The significant shift in voltages in the transgenic rice samples compared with that of the wild-type rice samples indicated the capability of RapiSense to detect transgene mRNA transcripts (Fig. 7D). Collectively, these results demonstrate that the AEM-based biosensor prototype, RapiSense, is capable of detecting its gene targets and is user-friendly for practical applications in actual transgenic plant samples.

4. Discussion

Nucleic acid biosensors have important applications in a wide range of fields, including disease diagnosis, environmental monitoring, and food safety, and offer sensitivity and specificity for more accurate results. In this study, the novel AEM-based nucleic acid biosensor monitored changes in the CVC after the surface-functionalized probes were bound to their specific gene targets, increasing the negatively charged nucleic acid molecules on the positively charged anion exchange nanomembrane and hindering electroconvection to increase the voltage thresholds for ion entry into the membrane (Sensale et al., 2021). We detected gene markers in GMOs as surrogate targets to develop a novel membrane nucleic acid biosensor into a nucleic acid diagnostic platform that offers significant advantages. First, by using GMOs as surrogate targets instead of working directly with hazardous pathogens or infectious agents, real biological samples can be safely analyzed without handling potentially harmful biological materials. Additionally, our efforts to detect these GMO crops are crucial for ensuring food safety so that individuals can make informed decisions with the increasing presence of GMOs in the global food supply.

Due to the finite amounts of single-stranded DNA probes functionalized on the membrane surface, there should be an upper limit for the probes to bind to the complementary gene targets. Within the range of gene target concentrations tested (8 nM to 16 μM, Fig. 3C), the saturation concentration of the measured voltage shift for the membrane biosensor was observed with the gene target at 8 μM and 16 μM, supporting an upper limit of ΔV posed by the amounts of functionalized probes to specifically bind their gene targets. When the membrane biosensor was built using a smaller membrane (0.12 mm^2) and compared to a larger membrane (0.35 mm^2), the reduced amounts of probes functionalized on the smaller membrane most likely caused a reduction in the saturation concentration. Interestingly, biosensors with smaller membranes also showed improved sensitivity compared to larger membranes (Fig. 5B) similar to the 4–5 folds improvement

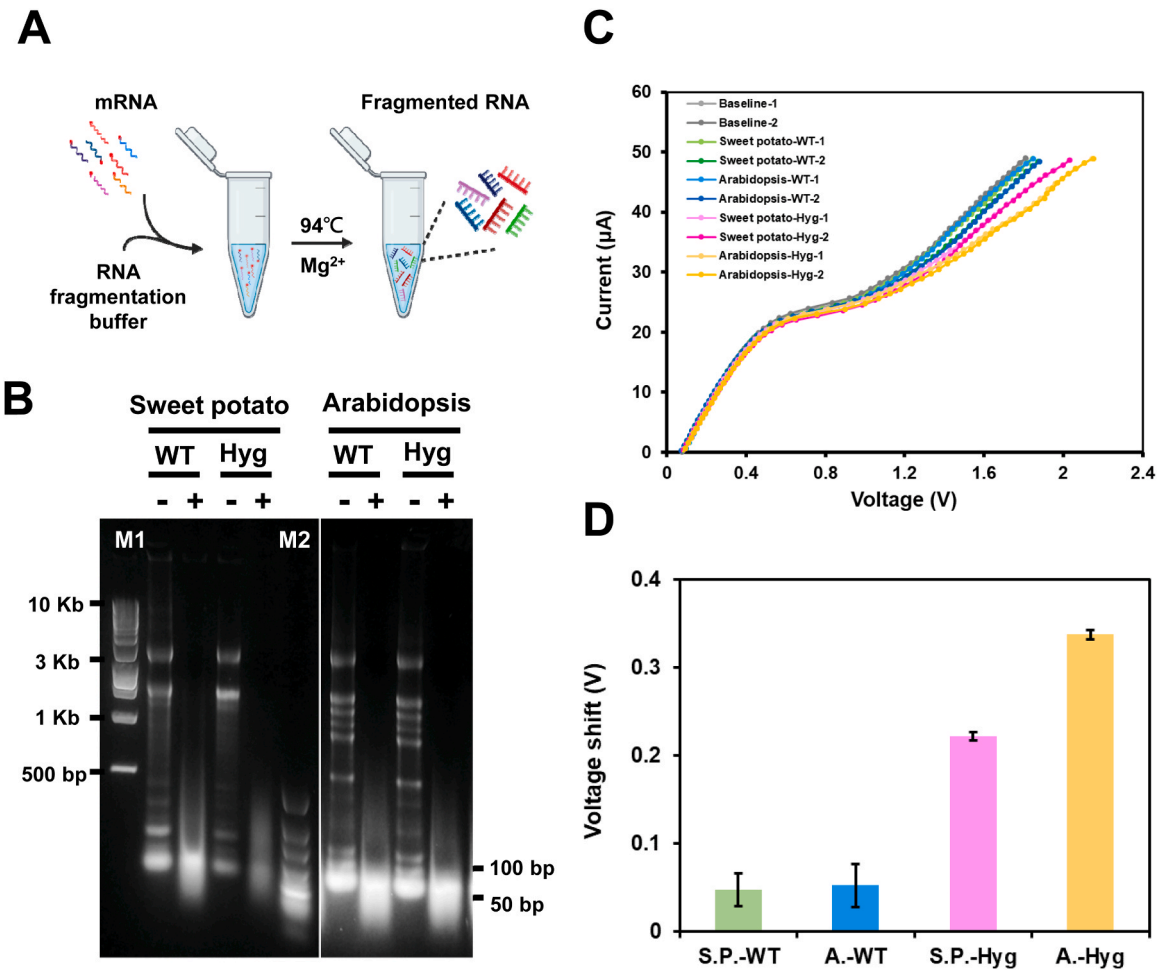

Fig. 6. The fragmented RNA from plant samples was detected by the membrane sensor. (A) Schematic diagram of mRNA fragmentation using NEBNext magnesium RNA fragmentation buffer for the 94 ℃ treatment. (B) Size distribution of fragmented or non-fragmented total RNA from wild-type or transgenic sweet potato or Arabidopsis, respectively. The sizes of the makers are indicated. (C) Current–voltage characteristics of fragmented RNA of wild-type (WT) and transgenic plants (Hyg) from sweet potato or Arabidopsis were recorded in each detection process. The results showed that the transgenic sweet potato and Arabidopsis have higher voltage shifts than the WT. (D) Bar diagram showing voltage shift from baseline in four fragmentated RNAs from sweet potato (S.P.) and Arabidopsis (A.).

reported in a previous study (Senapati et al., 2014). Although building biosensors with smaller membranes is advantageous, it is technically more challenging to cut and embed AEM on the biosensors with a surface sizes of less than 1 mm^2. Alternatively, a 2-hydroxyethyl methacrylate (HEMA)-based hydrogel polymer AEM membrane (Chuang et al., 2020) has been developed to allow *in situ* membrane synthesis in a small preformed hole on a microfluidic sensor chip to allow the scale-up production of the sensor chips with improved sensitivity.

Nucleic acid samples were hybridized to a membrane biosensor at room temperature to simplify the nucleic acid detection process. Therefore, evaluating the effects of probe hybridization under reduced stringency at a temperature at least 20°C lower than its melting temperature is important. The reduction in the measured voltage shift for mismatched targets with one to three mismatches was 40–70% (Fig. 4C), similar to the 30–50% reduction in target hybridization measured in a previous study using surface plasmon resonance with specific probes functionalized on a gold surface (Peterson et al., 2002). The results with mismatched targets suggest that the functionalized probe on the AEM biosensor may still detect gene target variants with few nucleotide differences at reduced levels at room temperature, suggesting its capability to detect closely related gene variants when the probes are selected from shared sequences.

Various fragmentation methods can be used to reduce the formation of secondary and tertiary structures in long RNA molecules and improve the hybridization efficiency. This includes chemical, physical (acoustic shearing/sonication/nebulization), and enzymatic fragmentation (Boone et al., 2018) to reduce the sizes of the RNAs and DNAs used in probe hybridization. A reduction in target length can result in increased hybridization efficiency and reduced false-negative signals, but it is essential to avoid making the fragments excessively short as this may instead lead to an increase in false-positive signals (Liu et al., 2007). In this study, we used chemical fragmentation in the presence of magnesium ions at high temperatures to generate RNA fragments of predominantly 50–100 nt in size to significantly improve their detection with a membrane biosensor. Although this approach requires an additional purification step to remove magnesium ions before the fragmented RNAs can be used for probe hybridization, it is important to visually confirm the resulting RNA fragment sizes. Alternatively, acoustic shearing/sonication can be used to generate RNA fragments for subsequent biosensor detection without additional purification steps. Ramshani *et al.* (Ramshani et al., 2021) showed that an AEM-membrane biosensor could also be utilized for protein detection using a membrane-functionalized antibody for the target protein along with a second reporter antibody conjugated with negatively charged silica nanoparticles in a sandwich scheme. Because the binding of fragmented RNAs to the complementary probes and the binding of target proteins to the specific antibodies are both performed under PBS-buffered physiological conditions, it is possible to create multiplexed AEM-membrane

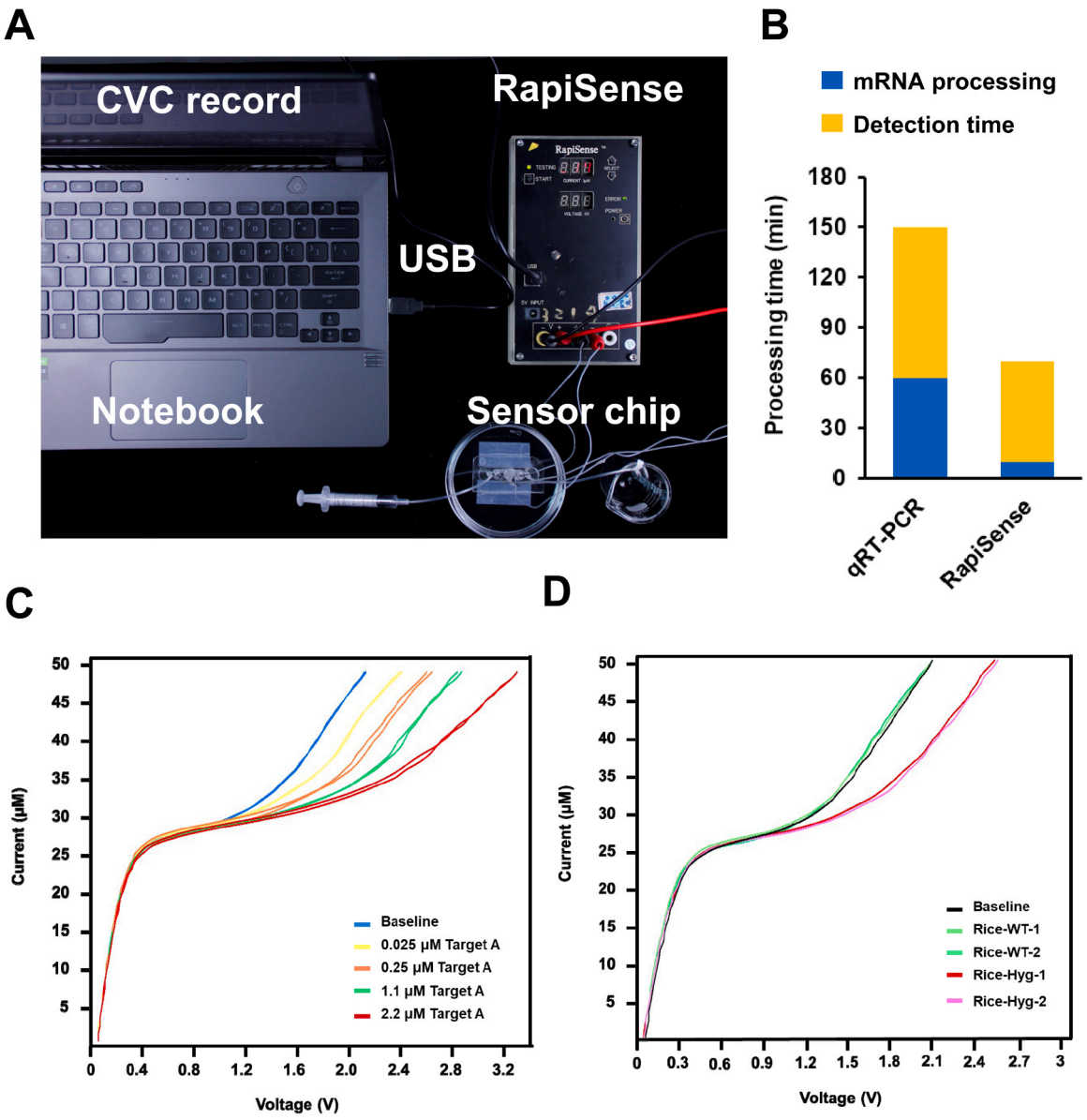

Fig. 7. The fragmented rice RNA was detected by RapiSense. (A) Photograph of the portable prototype and disposable membrane chip device. (B) The bar diagram illustrates the superior speed of the RapiSense detection system compared to the traditional method, qRT-PCR method. (C) Current–voltage characteristics of probe A-conjugated membrane sensor that targets the hygromycin resistance gene. The current-voltage of various target A single strand DNA concentrations was detected using RapiSense, with regenerated single strand DNA as the baseline. (D) Current-voltage characteristics of fragmented RNA of wild-type (WT) and transgenic rice (Hyg). Error bars indicate the standard deviations of three replicate experiments.

biosensors to create multiplexed AEM-membrane biosensors to simultaneously detect target proteins and unamplified RNAs in the same biological sample for further development, making the RapiSense biosensor system more useful and versatile than the current study reported here.

5. Conclusion

Our research advances the field of GM crop detection by introducing a portable biosensing platform, RapiSense for RNA detection. This AEM-based biosensor leverages the ion-depletion action of an anion-exchange membrane sensor to produce a voltage shift upon the hybridization of DNA/RNA targets with the DNA probe. We specifically tailored probes for detecting of the hygromycin phosphotransferase gene, a selection marker of antibiotic resistance, and demonstrated the capability to quantify a range of complementary targets effectively, with a range of ~1 nM to ~10 μM. Biosensors can discriminate against non-specific or nucleotide-mismatched targets. The successful detection of complementary DNA targets and fragmented RNA samples from transgenic sweet potato, Arabidopsis, and rice demonstrated the practicality of the RapiSense device. We anticipate that this breakthrough will alleviate the public concerns regarding GM crops by offering a convenient and effective tool for on-the-spot GM crop detection. Future research will explore the further refinement and commercial scalability of RapiSense, with the ultimate goal of fostering informed consumer choices and ethical food production practices.

CRediT authorship contribution statement

Chang Hsueh-Chia: Writing – review & editing, Supervision, Conceptualization. **Senapati Satyajyoti:** Writing – review & editing, Methodology, Data curation, Conceptualization. **Huang Li-Fen:** Writing – review & editing, Supervision, Project administration, Funding acquisition, Conceptualization. **Sun Yi-Ming:** Writing – review &

editing, Supervision, Resources. **Huang Wen-Shan:** Validation, Data curation. **Lin Yi-Nan:** Writing – review & editing, Supervision, Investigation. **Huang Chun-Kai:** Writing – original draft, Methodology, Investigation, Data curation.

Declaration of Competing Interest

The authors declare no competing financial interest.

Data availability

Data will be made available on request.

Acknowledgments

The authors gratefully acknowledge the financial support from the Far Eastern Y. Z. Hsu Science and Technology Memorial Foundation and Far Eastern Memorial Foundation. Transgenic plants used in this study were kindly provided by Dr. Chung-An Lu from the Department of Life Sciences, National Central University provided the transgenic plants used in this study. Additional recognition is extended to Rose Doerfler and Krishna Pratama for their contributions to the schematic representation of the nucleic acid detection biosensor system.

Appendix A. Supporting information

Supplementary data associated with this article can be found in the online version at doi:10.1016/j.jbiotec.2024.02.002.

References

Alizar, U., Lee, Y.H., Musa, A., Lau, H.-Y., Zamri, I., Tan, L.L., 2014. A regenerable screen-printed DNA biosensor based on acrylic microsphere–gold nanoparticle composite for genetically modified soybean determination. Sens. Actuators B: Chem. 190, 694–701.

Babin, A., Nawrot-Esposito, M.P., Gallet, A., Gatti, J.L., Poirie, M., 2020. Differential side-effects of Bacillus thuringiensis bioinsecticide on non-target Drosophila flies. Sci. Rep. 10, 16241.

Benbrook, C.M., 2016. Trends in glyphosate herbicide use in the United States and globally. Environ. Sci. Eur. 28, 3.

Beyer, P., 2010. Golden Rice and 'Golden' crops for human nutrition. New Biotechnol. 27, 478–481.

Boone, M., De Koker, A., Callewaert, N., 2018. Capturing the 'ome': the expanding molecular toolbox for RNA and DNA library construction. Nucleic Acids Res. 46, 2701–2721.

Chang, H.C., Demekhin, E.A., Shelistov, V.S., 2012. Competition between Dukhin's and Rubinstein's electrokinetic modes. Phys. Rev. E 86, 046319.

Charlebois, I., Gravel, C., Arrad, N., Boissinot, M., Bergeron, M.G., Leclerc, M., 2013. Impact of DNA sequence and oligonucleotide length on a polythiophene-based fluorescent DNA biosensor. Macromol. Biosci. 13, 717–722.

Chuang, J.N., Diao, P.Y., Huang, W.S., Huang, L.F., Senapati, S., Chang, H.C., Sun, Y.M., 2020. Novel homogeneous anion exchange membranes for reproducible and sensitive nucleic acid detection via current-voltage characteristic measurement. ACS Appl. Mater. Interfaces 12, 54459–54472.

Do, D.D., 1998. Adsorption Analysis: Equilibria and Kinetics, Chemical Engineer Series, vol. 2. Imperial College Press, London.

Dong, S., Liu, Y., Zhang, X., Xu, C., Liu, X., Zhang, C., 2019. Development of an immunochromatographic assay for the specific detection of Bacillus thuringiensis (Bt) Cry1Ab toxin. Anal. Biochem. 567, 1–7.

Egatz-Gomez, A., Wang, C., Klacsmann, F., Pan, Z., Marczak, S., Wang, Y., Sun, G., Senapati, S., Chang, H.C., 2016. Future microfluidic and nanofluidic modular platforms for nucleic acid liquid biopsy in precision medicine. Biomicrofluidics 10, 032902.

Gao, H., Cui, D., Zhai, S., Yang, Y., Wu, Y., Yan, X., Wu, G., 2022. A label-free electrochemical impedimetric DNA biosensor for genetically modified soybean detection based on gold carbon dots. Mikrochim Acta 189, 216.

Garcia-Martinez, G., Bustabad, E.A., Perrot, H., Gabrielli, C., Bucur, B., Lazerges, M., Rose, D., Rodriguez-Pardo, L., Farina, J., Compere, C., Vives, A.A., 2011. Development of a mass sensitive quartz crystal microbalance (QCM)-based DNA biosensor using a 50 MHz electronic oscillator circuit. Sens. (Basel) 11, 7656–7664.

Hendling, M., Barišić, I., 2019. In-silico design of DNA oligonucleotides: challenges and approaches. Comput. Struct. Biotechnol. J. 17, 1056–1065.

Huang, C.K., Lo, P.C., Huang, L.F., Wu, S.J., Yeh, C.H., Lu, C.A., 2015. A single-repeat MYB transcription repressor, MYBH, participates in regulation of leaf senescence in Arabidopsis. Plant Mol. Biol. 88, 269–286.

Huang, C.K., Sie, Y.S., Chen, Y.F., Huang, T.S., Lu, C.A., 2016. Two highly similar DEAD box proteins, OsRH2 and OsRH34, homologous to eukaryotic initiation factor 4AIII, play roles of the exon junction complex in regulating growth and development in rice. BMC Plant Biol. 16, 84.

Klumper, W., Qaim, M., 2014. A meta-analysis of the impacts of genetically modified crops. PLoS One 9, e111629.

Lee, H.-J., Hong, M.-K., Han, S.-D., Moon, S.-H., 2008. Influence of the heterogeneous structure on the electrochemical properties of anion exchange membranes. J. Membr. Sci. 320, 549–555.

Lin, A.A., Sastri, V.R., Tesoro, G., Reiser, A., Eachus, R., 1988. On the crosslinking mechanism of benzophenone-containing polyimides. Macromolecules 21, 1165–1169.

Liu, W.T., Guo, H., Wu, J.H., 2007. Effects of target length on the hybridization efficiency and specificity of rRNA-based oligonucleotide microarrays. Appl. Environ. Microbiol. 73, 73–82.

Mallory-Smith, C., Zapiola, M., 2008. Gene flow from glyphosate-resistant crops. Pest Manag. Sci. 64, 428–440.

Marvier, M., McCreedy, C., Regetz, J., Kareiva, P., 2007. A meta-analysis of effects of Bt cotton and maize on nontarget invertebrates. Science 316, 1475–1477.

Mehlmann, M., Townsend, M.B., Stears, R.L., Kuchta, R.D., Rowlen, K.L., 2005. Optimization of fragmentation conditions for microarray analysis of viral RNA. Anal. Biochem. 347, 316–323.

Miki, B., McHugh, S., 2004. Selectable marker genes in transgenic plants: applications, alternatives and biosafety. J. Biotechnol. 107, 193–232.

Nielsen, K.M., Bones, A.M., Smalla, K., van Elsas, J.D., 1998. Horizontal gene transfer from transgenic plants to terrestrial bacteria–a rare event? FEMS Microbiol. Rev. 22, 79–103.

Peterson, A.W., Wolf, L.K., Georgiadis, R.M., 2002. Hybridization of mismatched or partially matched DNA at surfaces. J. Am. Chem. Soc. 124, 14601–14607.

Philips, J.G., Martin-Avila, E., Robold, A.V., 2022. Horizontal gene transfer from genetically modified plants - regulatory considerations. Front. Bioeng. Biotechnol. 10, 971402.

Phuong, D.T., 2015. Genetically modified organism (GMO) detection by biosensor based on SWCNT material. Curr. Appl. Phys. 15, 397–401.

Ramshani, Z., Fan, F., Wei, A., Romanello-Giroud-Joaquim, M., Gil, C.H., George, M., Yoder, M.C., Hanjaya-Putra, D., Senapati, S., Chang, H.C., 2021. A multiplexed immuno-sensor for on-line and automated monitoring of tissue culture protein biomarkers. Talanta 225, 122021.

Ramshani, Z., Zhang, C., Richards, K., Chen, L., Xu, G., Stiles, B.L., Hill, R., Senapati, S., Go, D.B., Chang, H.C., 2019. Extracellular vesicle microRNA quantification from plasma using an integrated microfluidic device. Commun. Biol. 2, 189.

Randhawa, G.J., Chhabra, R., Singh, M., 2009. Multiplex PCR-based simultaneous amplification of selectable marker and reporter genes for the screening of genetically modified crops. J. Agric. Food Chem. 57, 5167–5172.

Rubio-Infante, N., Moreno-Fierros, L., 2016. An overview of the safety and biological effects of Bacillus thuringiensis Cry toxins in mammals. J. Appl. Toxicol. 36, 630–648.

Ruuskanen, S., Fuchs, B., Nissinen, R., Puigbo, P., Rainio, M., Saikkonen, K., Helander, M., 2023. Ecosystem consequences of herbicides: the role of microbiome. Trends Ecol. Evol. 38, 35–43.

Senapati, S., Slouka, Z., Shah, S.S., Behura, S.K., Shi, Z., Stack, M.S., Severson, D.W., Chang, H.C., 2014. An ion-exchange nanomembrane sensor for detection of nucleic acids using a surface charge inversion phenomenon. Biosens. Bioelectron. 60, 92–100.

Sensale, S., Ramshani, Z., Senapati, S., Chang, H.C., 2021. Universal features of non-equilibrium ionic currents through perm-selective membranes: gating by charged nanoparticles/macromolecules for robust biosensing applications. J. Phys. Chem. B 125, 1906–1915.

Shelton, A.M., Hossain, M.J., Paranjape, V., Azad, A.K., Rahman, M.L., Khan, A., Prodhan, M.Z.H., Rashid, M.A., Majumder, R., Hossain, M.A., Hussain, S.S., Huesing, J.E., McCandless, L., 2018. Bt eggplant project in Bangladesh: history, present status, and future direction. Front. Bioeng. Biotechnol. 6, 106.

Sigal, G.B., Bamdad, C., Barberis, A., Strominger, J., Whitesides, G.M., 1996. A self-assembled monolayer for the binding and study of histidine-tagged proteins by surface plasmon resonance. Anal. Chem. 68, 490–497.

Slouka, Z., Senapati, S., Shah, S., Lawler, R., Shi, Z., Stack, M.S., Chang, H.C., 2015. Integrated, DC voltage-driven nucleic acid diagnostic platform for real sample analysis: Detection of oral cancer. Talanta 145, 35–42.

Slouka, Z., Senapati, S., Yan, Y., Chang, H.-C., 2013. Charge inversion, water splitting, and vortex suppression due to DNA sorption on ion-selective membranes and their ion-current signatures. Langmuir 29, 8275–8283.

Sorgenfrei, S., Chiu, C.Y., Gonzalez Jr., R.L., Yu, Y.J., Kim, P., Nuckolls, C., Shepard, K.L., 2011. Label-free single-molecule detection of DNA-hybridization kinetics with a carbon nanotube field-effect transistor. Nat. Nanotechnol. 6, 126–132.

Suzuki, S., Ono, N., Furusawa, C., Kashiwagi, A., Yomo, T., 2007. Experimental optimization of probe length to increase the sequence specificity of high-density oligonucleotide microarrays. BMC Genom. 8, 373.

Taller, D., Richards, K., Slouka, Z., Senapati, S., Hill, R., Go, D.B., Chang, H.C., 2015. On-chip surface acoustic wave lysis and ion-exchange nanomembrane detection of exosomal RNA for pancreatic cancer study and diagnosis. Lab Chip 15, 1656–1666.

Tripathi, S., Suzuki, J., Gonsalves, D., 2007. Development of genetically engineered resistant papaya for papaya ringspot virus in a timely manner: a comprehensive and successful approach. Methods Mol. Biol. 354, 197–240.

Un Jan Contreras, S., Gardner, C.M., 2022. Environmental fate and behaviour of antibiotic resistance genes and small interference RNAs released from genetically modified crops. J. Appl. Microbiol 133, 2877–2892.

Wang, H., Wu, Y., Zhang, Y., Yang, J., Fan, W., Zhang, H., Zhao, S., Yuan, L., Zhang, P., 2019. CRISPR/Cas9-based mutagenesis of starch biosynthetic genes in sweet potato (ipomoea batatas) for the improvement of starch quality. Int J. Mol. Sci. 20.
Wetmur, J.G., 1991. DNA probes: applications of the principles of nucleic acid hybridization. Crit. Rev. Biochem. Mol. Biol. 26, 227–259.
Wu, Y., Li, J., Wang, Y., Li, X., Li, Y., Zhu, L., Li, J., Wu, G., 2016. Development and application of a general plasmid reference material for GMO screening. Plasmid 87-88, 28–36.
Ye, X., Al-Babili, S., Kloti, A., Zhang, J., Lucca, P., Beyer, P., Potrykus, I., 2000. Engineering the provitamin A (beta-carotene) biosynthetic pathway into (carotenoid-free) rice endosperm. Science 287, 303–305.
Yin, Z., Ramshani, Z., Waggoner, J.J., Pinsky, B.A., Senapati, S., Chang, H.-C., 2020. A non-optical multiplexed PCR diagnostic platform for serotype-specific detection of dengue virus. Sens. Actuators B: Chem. 310, 127854.
Zhang, Y., Zhang, W., Liu, Y., Wang, J., Wang, G., Liu, Y., 2016. Development of monoclonal antibody-based sensitive ELISA for the determination of Cry1Ie protein in transgenic plant. Anal. Bioanal. Chem. 408, 8231–8239.